Article

A Flow-Speed Model for Motorways in England: Analysis Under Various Weather Conditions

Ye Liu [1], Haibo Chen [1], Chuhan Yin [1], Vivi Michalaki [2], Phillip Proctor [2], Gavin Rowley [2], Xiaowei Wang [3,*] and Hongyuan Wei [3]

1   Institute for Transport Studies, University of Leeds, Leeds LS2 9JT, UK
2   National Highways, Temple Quay House, 2 The Square, Bristol BS1 6HA, UK
3   CATARC Automotive Research and Inspection Centre (Tianjin) Co., Ltd., Tianjin 300300, China
*   Correspondence: wangxiaowei@catarc.ac.cn

Abstract: This work proposes a single regime speed–flow model to fit the speed–flow relationship on the M25, London's main motorway which is recurrently congested, especially near Heathrow Airport. The proposed model had a better performance compared with the existing classic models. A whole year's field data on various sites of the M25 motorway were collected by the National Highways MIDAS (Motorway Incident Detection and Automatic Signalling) system and analysed. The proposed model was fitter on both four-lane and lane-by-lane conditions than the existing models, in terms of lower relative error and RMSE values and higher R^2 values (minimum $R^2 = 0.79$), which means the proposed model captured the speed–flow relationship better. In addition, the proposed model was used to fit traffic characteristics under different weather conditions and decided the threshold of the CM algorithms using the Gaussian function. The results showed that both free-flow speed and road capacity were significantly reduced by up to 7% and 11%, respectively, under different rainfall conditions, and that congestion management should be triggered in advance on rainy days. Further analysis of extensive data over a wider space and time is required to test the transferability of these findings to other contexts.

Keywords: single-regime model; speed–flow relationship; traffic flow; traffic speed; M25 motorway

1. Introduction

Speed–flow models represent the interaction between speed and traffic flow, which can be used to predict the critical values of road traffic speed and flow, thus playing a crucial role in transportation planning [1–4]. When the critical values of traffic speed or flow are surpassed, flow breakdown and stop–go waves occur. Flow breakdown diminishes the effective capacity and traffic speed, leading to delays [5–8]. In addition, stop–go waves of moving congestion tend to form, resulting in rapid changes in local speed, which disrupt traffic flow, waste energy, emit more emissions, and create collision hazards [9,10]. Today, more and more of the world's highways are equipped with intelligent automatic traffic management systems to smooth traffic flow and reduce congestion [11,12].

On England's motorways, two traffic management algorithms, namely, congestion management (CM) and queue protection (QP), are used as part of the operation of smart motorways. Although the smart automatic traffic management system has been applied to England's motorways, congestion occurs from time to time, especially on the M25. The M25, encircling London, is recognised as one of the busiest motorways in the country, with an average daily traffic volume of 209,368 vehicles recorded in 2023 on the segment near

Heathrow Airport (Junctions 14 and 15) [13]. Previously, Taylor et al. [4] attempted to determine the relationship between traffic speed and flow for the M6 and M60 motorways in England, but there has been no study on the specific speed–flow relationship of the M25 motorway. In addition, the M25 was chosen in this study due to the following factors: (1) the current work focuses on the effect of weather factors on congestion; and (2) the M25 can serve as a representative case for congested UK motorway, given its high traffic volume and frequent congestion. Therefore, it is necessary to better understand the relationship between traffic flow and speed on the M25 motorway and further optimise the CM algorithms to mitigate congestion.

Traffic flow characteristics change under different weather conditions because of different driver behaviours, and how they are affected is different. Rainfall is the most common adverse weather in the UK, and both the free-flow speed and speed-at-capacity of the motorway are impacted on rainy days, especially on heavy rainy days. Hranac [14] studied the freeway in the United States and demonstrated that light rain reduced speed and flow by 2–4% and 10–11%, respectively. Akin et al. [15] observed that rainfall reduced speed by 8–12% and capacity by 7–8% on an urban freeway in Turkey. Xu et al. [16] reported that the reduction of the free-flow speed on freeways under light and heavy rain was 2–13% and 3–17%. Recently, Salvi et al. [17] analysed the sensitivity of traffic speed to varying rainfall intensities across multiple road sections in Alabama, USA. They found that the extent of the reduction was influenced by the intensity of the rainfall, along with the free-flow speed of the road section and existing traffic volume. Nguyen et al. [18] applied a Vector Autoregressive Model to study how weather conditions influenced traffic flow. Their research indicated that weather conditions significantly affected traffic volume, with precipitation leading to notable reductions in traffic speed and flow. Yang and Qian [19] developed a data-driven approach to predict highway travel time, revealing that precipitation significantly increased travel times and reduced speeds. However, there is limited research on how weather conditions impact the UK motorway and on how to combine congestion management with weather conditions. Thus, it is necessary to analyse rainfall impacts on the M25 motorway and enhance the CM algorithm under rainfall conditions. The main contribution of this research is the development and validation of the proposed speed–flow model and its application to congestion management under different weather conditions on the M25 motorway.

2. Literature Review

2.1. Speed–Flow Model

According to the literature, single-regime models and multi-regime models are widely used to describe the relationship between speed and flow nowadays. As shown in Table 1, single-regime models may be classified into three types: generalised polynomial models, exponential models, and logarithmic models. The Greenshields model [20] is the most representative of the generalised polynomial models, which was first acquired by field data fitting. In addition, this category also contains the Pipes–Munjal model [21], the Drew model [22] and the modified Greenshields model [23]. Although the developed Pipes–Munjal model, Drew model and modified Greenshields model made an effort to advance the basic model by incorporating new parameters, the curves are insufficient to accurately represent the actual data under various traffic situations. The Underwood model [24] is a representation of the generalised exponential models, including the Newell model [25], Northwestern model [26], Kerner and Konhauser model [27], and the Logistic 3PL model [28], as listed in Table 1. This category of models presents a satisfactory performance in low-density conditions [25,28]. The primary shortcomings, however, are the prediction ability of the infinity jam condition and the optimum value from field data. The

Greenberg model [29] is a generalised logarithmic function, which improves performance as the traffic flow increases. However, under this model, the free-flow speed approaches towards infinity. Additionally, optimum speed and jam density are difficult to determine using empirical data.

Table 1. Single regime models.

Single-Regime Models	Categories	Function
[20]	Generalised polynomials	$v = v_f\left(1 - \frac{k}{k_j}\right)$
[22]	Generalised polynomials	$v = v_f\left(1 - \left(\frac{k}{k_j}\right)^{n+\frac{1}{2}}\right)$
[21]	Generalised polynomials	$v = v_f\left(1 - \left(\frac{k}{k_j}\right)^{n}\right),\ n > 1$
[30]	Generalised polynomials	$k = \frac{1}{c_1 + \frac{c_2}{v_f - v} + c_3 v}$
[23]	Generalised polynomials	$v = v_0 + \left(v_f - v_0\right)\left(1 - \frac{k}{k_j}\right)^{\alpha}$
[24]	Generalised exponent	$v = v_f \exp\left(-\frac{k}{k_j}\right)$
[27]	Generalised exponent	$v = v_f\left[1 - \exp\left(-\frac{Q}{v_f}\left(\frac{1}{k} - \frac{1}{k_c}\right)^2\right)\right]$
[26]	Generalised exponent	$v = v_f \exp\left(-\frac{1}{2}\left(\frac{k}{k_c}\right)^2\right)$
[27]	Generalised exponent	$v = v_f\left(\frac{1}{1+\exp\left(\frac{k/k_c - 0.25}{0.06}\right)} - 3.72 \times 10^{-6}\right)$
[28]	Generalised exponent	$v = \frac{v_f}{1+\exp\left(\frac{k-k_c}{\theta_1}\right)}$
[29]	Generalised logarithm	$v = v_c \log\frac{k_j}{k}$

Where v_f is free flow speed, v_c is the critical speed at the average maximum capacity, v_0 is the average speed at zero flow, k represents vehicle density, k_j is the congestion density, k_c is the density at critical speed, and θ_1 is the known flow.

Multi-regime models have been developed to compensate for the shortcomings of a single-regime model that cannot consistently match field data throughout the whole density range. The typical two-regime model considered the free-flow and congested-flow regimes [21–33], and the three-regime model [34] considered the transitional flow on extra based on the two-regime model. However, it has obvious drawbacks: it is hard to ascertain the precise number of regimes; it is unable to determine the breakpoint of the traffic flow; it is hard to determine the single regime used for a certain curve, and each regime unavoidably inherits the inherent issues in the chosen single-regime function. Recently, Lei et al. [35] developed a sparse Gaussian process regression model to formulate stochastic fundamental diagrams, which effectively captures the inherent variability in traffic flow and provides a more robust representation of speed–density relationships. Cheng et al. [36] developed a Bayesian calibration method using Gaussian Processes to model speed–density relationships, offering a flexible, non-parametric approach that accounts for uncertainties in traffic flow data.

The congestion management framework in the UK is based on identifying well-defined thresholds for the congestion phase, determined by the turning point within a single-regime model. However, multi-regime models segment traffic conditions into multiple regimes, introducing additional turning points and potential discontinuities, which complicate threshold identification and render these models unsuitable for the UK's congestion management framework. The single-regime models, while widely used, struggle to capture real-world traffic data under a variety of conditions, particularly under high-density or congested conditions. Therefore, this study aims to emphasise the development of a

single-regime model to address the limitations of existing models in order to capture the relationship between speed and flow, especially under congested conditions.

2.2. Precipitation Impacts on Speed–Flow Model

The effect of precipitation on traffic flow and speed has been widely studied, and almost all studies have found that precipitation reduces speed and road capacity. Chin et al. [37] found that rain had the greatest effect on road capacity reduction compared with snow and ice, and the heavier the rainfall, the greater the impact on capacity and speed. Rakha et al. [38] assessed the effects of rainfall on the highway based on different regions in the United States and discovered that rainfall reduced the free-flow speed and the speed at capacity by 6–9% and 8–14%, respectively. Additionally, rainfall had a 10–11% decrease in capacity. Akin et al. [15] studied both the weather conditions and surface conditions of two main urban freeways in Turkey and found that rainfall led to an 8–12% reduction in free-flow speed and a 7–8% reduction in capacity. Heshami et al. [39] studied the basic diagram parameters of various weather conditions of a Canadian highway and found that snow had a greater negative impact on traffic conditions, reducing speed and flow by 10.9% and 14%, respectively. In addition, some studies found that the reduction in both flow and speed would be greater when precipitation intensities increased. Table 2 lists the decreased proportion of speed and flow in previous studies which classified different precipitation intensities into four types, including light and heavy rain and light and heavy snow. In Table 2, regional differences can be observed in how precipitation impacts traffic. Snow had the greatest impact in regions like Alberta, Canada, with speed reductions of up to 35% during heavy snow, reflecting extreme weather challenges. Rain impacts varied by adaptation levels, with regions like Seattle showing smaller reductions during light rain (2–4%) compared to South Korea, where even light rain reduced speed by 5%. These variations indicate that, in addition to precipitation, local infrastructure, climate adaptation, and driving behaviours play a role in traffic flow and capacity.

Table 2. Proportion of decrease in speed and capacity under different precipitation intensities.

Reference	Area	Rain				Snow			
		Light Rain		Heavy Rain		Light Snow		Heavy Snow	
		Speed	Capacity	Speed	Capacity	Speed	Capacity	Speed	Capacity
[40]	Alberta, Canada	2–14%	~15%	5–17%	~15%	3–10%	5–10%	20–35%	25–30%
[41]	Minneapolis, USA	/	/	4–7%	10–17%	/	/	11–15%	19–27%
[42]	South Korea	5%	4–7%	8%	~14%	/	/	/	/
[43]	Ames, USA	2–4%	2–7%	6%	14%	4–8%	4–10%	13%	22%
[14]	Seattle, USA	2–4%	10–11%	/	/	5–16%	12–20%	/	/
[44]	Belgium	/	/	5–8%	5–8%	/	/	/	/
[45]	Louisville, USA	3%	7%	7%	17%	/	/	/	/

3. Methodology

3.1. Proposed Speed–Flow Model

The proposed model was created based on the existing Underwood model [24,46] and was used to simulate a traffic speed–flow relationship based on observations of speed–flow scatter plots at 150 locations along the M25 motorway. It was assumed that the studied site presented clear congestion conditions. This model is expressed by the following equation. The four parameters (a, c_1, c_2, and c_3) were selected to ensure the model can capture key traffic characteristics: a scales the flow variable, c_1 and c_2 control the curve's shape to reflect

transitions in traffic states, and c_3 balances free-flow and congested conditions. These parameters make the model flexible and accurate for real-world data.

$$v = v_0 \left[c_1 \cdot \exp\left(-\left(\frac{f}{av} \right)^{c_2} \right) + (1 - c_1) \cdot \exp\left(-\left(\frac{f}{av} \right)^{c_3} \right) \right] \tag{1}$$

where v is the actual average speed, v_0 is the average speed at zero flow, f is the actual flow, a, c_1, c_2, c_3 are parameters of the model ($0 \leq c_1 \leq 1$, c_2, $c_3 \geq 0$), which were determined through nonlinear curve fitting using MATLAB's lsqcurvefit function. The outliers identified using the Interquartile Range method were flagged and excluded to ensure the dataset's consistency and reliability. It follows the criteria: (1) the proposed exponential function closely matches real-world data on traffic speed and flow; (2) it is a single-regime model but reflects a primary phenomenon; (3) in comparison to the existing classic models, the proposed model presents better results in terms of the R^2 coefficient, relative error, and root mean-squared error (RMSE).

3.2. Model Analysis with Varying Important Parameters

Figure 1 illustrates a set of speed–flow curves generated by altering one parameter at a time while maintaining the values of the other parameters constant. As shown in Figure 1a, parameter c_1 has a significant effect on both the speed of the free-flow zone and the turning points of the speed–flow relationship. When the c_2, c_3 and a parameters remained at 3, 5 and 7.69, respectively, the average speed at zero flow decreased significantly as the parameter c_1 increased from 0.84 to 0.90. As illustrated in Figure 1b, parameter c_2 has a large effect on congested flow (the turning point) but has a minimal influence on the flow–speed zone. When c_1, c_3 and a were kept at 0.90, 5 and 7.69, respectively, the average speed at zero flow stayed almost constant with increasing c_2, whilst the turning point of the speed–flow relationship decreased dramatically. Generally, the turning point of the traffic speed–flow relationship remains stable under normal situations; however, there will be significant changes if the road conditions or traffic situation change. The values of $c_1 = 0.9$, $c_2 = 3$, $c_3 = 5$, and $a = 7.69$ are not constant for the 150 local observation points on the M25. These parameters varied across local locations due to the different traffic conditions, such as congestion levels and geometric features of the road.
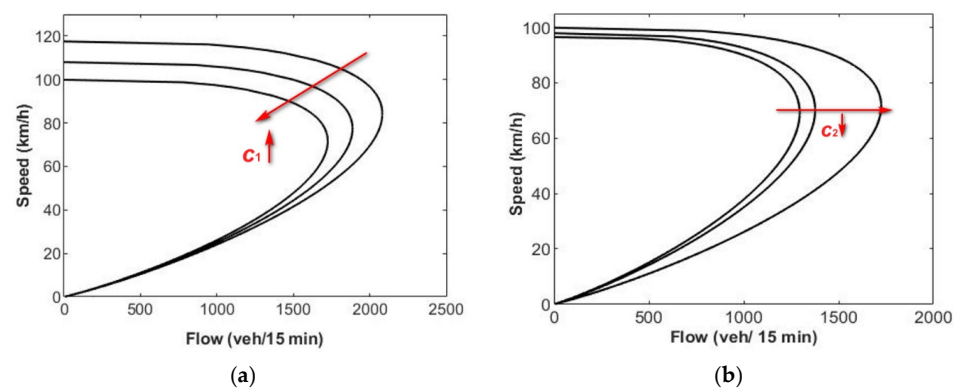

(a) (b)

Figure 1. Effects of varying crucial parameters, (**a**) *c₁* and (**b**) *c₂*, on the speed–flow relationship.

3.3. Speed–Flow Relationship Under Different Precipitation

According to previous studies, precipitation has been proven to have an effect on both traffic speed and road capacity, which inevitably influences the relationship between speed and flow. Figure 2 represents the traffic flow and speed of the M25 motorway on two random days: one of them a sunny day and the other a heavy rainy day. It was shown that both traffic flow and speed under heavy rain had a significant reduction, which means

the traffic speed–flow relationship is different under sunny days and under rainy days on the M25 motorway. This work used the proposed speed–flow model to fit the traffic speed–flow and capture the relationship between the speed and flow of the M25 motorway under different weather conditions.
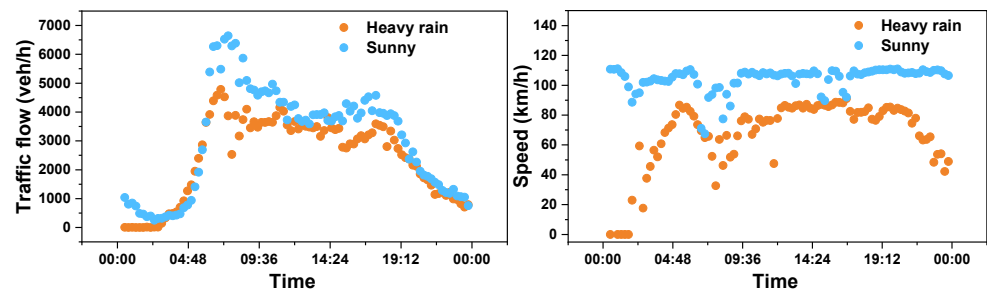

Figure 2. Traffic flow and speed under different weather conditions.

4. Results and Discussion

4.1. Data Collection

A 99-km transport route running along the M25 motorway (see Figure 3) was chosen for the analysis of congested traffic flow and speed relationship since this is one of the most important and busiest roads in England. The data were collected from the National Highways MIDAS (Motorway Incident Detection and Automatic Signalling) system, which gathers data from inductive loop sites on each lane that are typically 400–500 m apart. These data are primarily utilised to monitor and control traffic signals in real time. It is general practice to calibrate a single-regime speed–flow curve for a location over 12 months, and thus, the 12-month period from 1 July 2018 to 30 June 2019 was employed in the current work. Traffic speed and flow of the M25 motorway were calculated with fifteen-minute observation intervals. This research was to examine the overall speed–flow correlation on the congested motorway network, so all data including the morning and evening rush hours for the whole year were analysed. The data were not filtered by weekday in order to offer a more comprehensive view of the relationships between the variables.
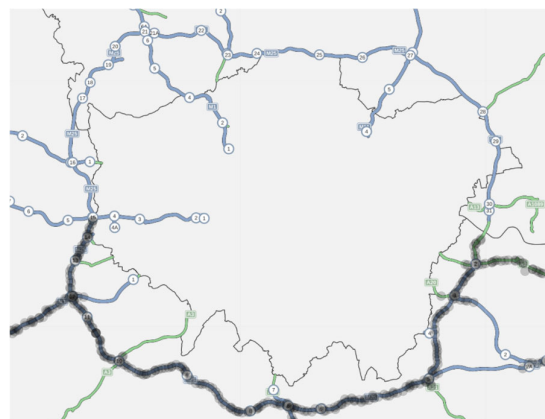

Figure 3. Road map running along the M25 motorway (dark colour).

4.2. Model Evaluation

In the current work, the existing single-regime speed–flow models and our proposed model were used to fit field data from 120 congested sites on the M25 motorway. Here, only models with better performance fitting to field data, including the Greenshields model, Northwestern model, Van Aerde model, and Underwood model, are presented to compare with our proposed model. Figure 4 illustrates some examples of these classic models and the proposed model for fitting field data from the M25 motorway. M25/4068 and

M25/4229A are located between junctions 1 and 2 and junctions 4 and 5, respectively. It can be observed that the proposed model can match the field data of the M25 motorway well under both free-flow and congested-flow situations. Among the five single-regime speed–flow models considered, our proposed model showed a better performance when compared to the other four models.
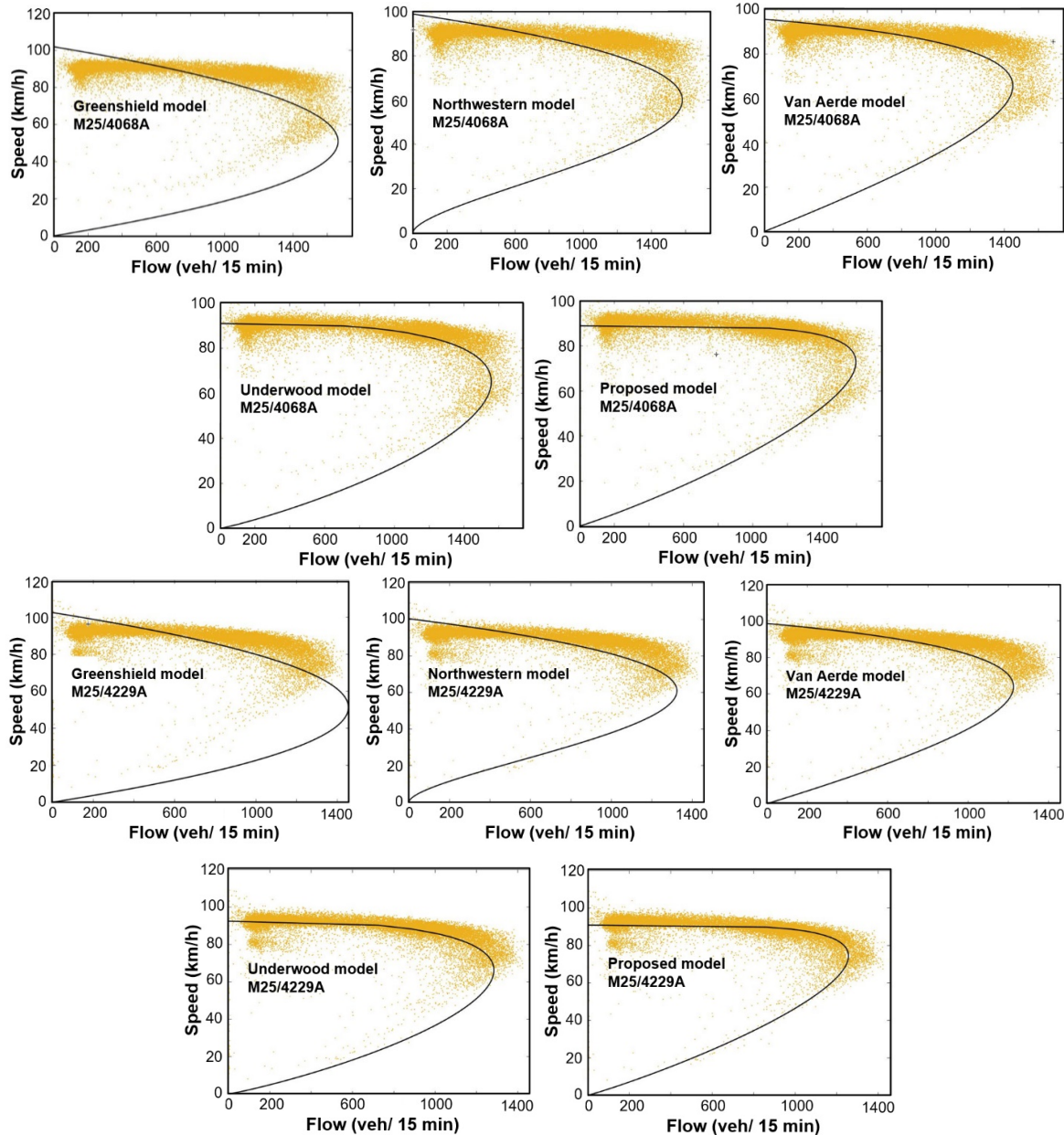

Figure 4. Performance of the classic model and our proposed model fitting to four-lane field data from various sites on the M25 motorway.

To assess how well a fitted model accounts for variance in the field data, the coefficient of R^2 is utilised as an indicator of goodness-of-fit. It is calculated by the following equation:

$$R^2 = 1 - \frac{\sum\left(f_o(v) - f_p(v)\right)^2}{\sum\left(f_o(v) - f_m(v)\right)^2} \tag{2}$$

where $f_r(v)$ refers to the observed field data, $f_p(v)$ denotes the predicted data according to the fitted curve, and $f_m(v)$ is the average value of the observed field data. The closer R^2 value to 1, the better the model fitted. Furthermore, according to

previous studies [47–50], R^2 is insufficient for determining which model is superior, and the relative error (*E*) and *RMSE* are introduced to quantify the closeness between the proposed model and other existing models due to the unsuitability of R^2 for comparative analysis, defined as Equations (3) and (4), respectively.

$$E = \frac{1}{n}\sum \left| \frac{f_o(v) - f_p(v)}{f_o(v)} \right| \tag{3}$$

$$RMSE = \frac{1}{n}\sqrt{n\sum_{i=1}^{n}(f_p - f_o)^2} \tag{4}$$

where $f_o(v)$ refers to the observed field data and $f_p(v)$ denotes the fitted curve's projected data. The closer the relative error and RMSE values are to zero, the better the model performance is. Table 3 shows the R^2 results for 20 randomly selected sites on the M25 motorway, given the limitations of publication space, and Table 4 summarises their *E* and *RMSE* results. It can be seen that the proposed model outperformed all other models, with a minimum R^2 value of 0.83 across the 20 randomly selected sites, clearly higher than the Greenshields, Northwestern, and Van Aerde models. Although Underwood's model performed relatively well, it was still outmatched by the proposed model in both R^2 and predictive accuracy. Additionally, the proposed model achieved smaller average relative error and RMSE, confirming its superior ability to capture the speed–flow relationship. However, in our research, it was found that the accuracy of our developed model tended to decline in situations with lighter motorway congestion. Nevertheless, compared to the classic models, its performance remained better than that of other classic models under such conditions. The mathematical complexity of the developed model may lead to increased computational cost, particularly in scenarios requiring real-time processing. Additionally, the current research focuses primarily on the M25 motorway, and we have not yet conducted studies on other highways. Therefore, the proposed model may have limitations in its applicability to highways with different traffic conditions and infrastructure.

Table 3. Results of data fitting for R^2 using the classic model and our proposed model.

Data Sites	Greenshields	Northwestern	Van Aerde	Underwood	The Proposed Model
	R2	R2	R2	R2	R2
M25/4055A	0.21	0.34	0.27	0.78	0.91
M25/4076A	0.39	0.44	0.21	0.83	0.85
M25/4097A	0.21	0.24	0.11	0.79	0.86
M25/4120A	0.17	0.17	0.26	0.79	0.89
M25/4139A	0.07	0.07	0.27	0.85	0.92
M25/4164A	0.23	0.23	0.11	0.77	0.84
M25/4193A	0.02	0.02	0.26	0.77	0.93
M25/4229A	0.07	0.07	0.06	0.85	0.92
M25/4259A	0.15	0.07	0.10	0.73	0.83
M25/4277A	0.07	0.07	0.10	0.78	0.85
M25/4296A	0.02	0.02	0.11	0.79	0.87
M25/4315A	0.07	0.07	0.21	0.78	0.90
M25/4332A	0.07	0.07	0.11	0.69	0.87
M25/4332A	0.04	0.04	0.27	0.81	0.92
M25/4358A	0.03	0.03	0.06	0.87	0.86
M25/4390A	0.11	0.11	0.07	0.75	0.91
M25/4409A	0.22	0.22	0.23	0.85	0.91
M25/4423A	0.06	0.06	0.02	0.75	0.85
M25/4442A	0.08	0.13	0.07	0.68	0.86
M25/4465A	0.14	0.16	0.24	0.69	0.86

Table 4. Results of data fitting for *E* and *RMSE* using the classic model and our proposed model.

Data Sites	Greenshields		Northwestern		Van Aerde		Underwood		The Proposed Model	
	E	*RMSE*	*E*	*RMSE*	*E*	*RMSE*	*E*	*RMSE*	*E*	*RMSE*
M25/4055A	0.51	338.63	0.28	309.93	0.33	246.54	0.21	6.54	0.15	4.70
M25/4076A	0.40	305.73	0.52	292.88	0.46	198.65	0.12	8.62	0.12	4.93
M25/4097A	0.53	397.12	0.37	391.80	0.32	263.45	0.14	7.65	0.12	5.42
M25/4120A	0.59	328.13	0.43	326.56	0.44	475.32	0.14	8.45	0.13	5.79
M25/4139A	0.46	297.85	0.30	297.86	0.31	168.25	0.17	10.35	0.16	6.20
M25/4164A	0.41	352.93	0.41	352.63	0.35	195.46	0.19	7.65	0.12	4.57
M25/4193A	0.43	302.99	0.31	302.99	0.32	203.65	0.19	8.65	0.11	4.98
M25/4229A	0.50	335.17	0.43	335.18	0.45	218.45	0.18	9.25	0.12	5.13
M25/4259A	0.48	208.11	0.47	207.95	0.49	205.36	0.21	7.54	0.15	5.78
M25/4277A	0.50	429.89	0.38	429.90	0.32	214.78	0.17	9.65	0.13	6.87
M25/4296A	0.54	419.00	0.35	419.01	0.32	221.54	0.19	8.25	0.17	7.23
M25/4315A	0.54	420.01	0.38	420.01	0.35	204.65	0.17	11.35	0.14	7.81
M25/4332A	0.35	390.13	0.32	390.13	0.36	204.35	0.16	12.45	0.15	6.68
M25/4358A	0.36	414.35	0.34	414.35	0.38	206.15	0.22	9.35	0.16	7.48
M25/4390A	0.42	432.36	0.38	432.37	0.38	145.67	0.21	10.45	0.15	7.71
M25/4409A	0.37	325.07	0.34	325.08	0.47	175.32	0.27	12.21	0.18	7.08
M25/4423A	0.44	338.54	0.39	338.54	0.42	142.56	0.25	9.78	0.17	6.03
M25/4442A	0.48	360.01	0.45	360.01	0.46	184.35	0.26	12.02	0.11	6.49
M25/4465A	0.46	338.63	0.42	338.63	0.42	201.32	0.30	11.38	0.17	7.93
M25/4479A	0.52	460.39	0.48	456.13	0.44	223.65	0.26	9.67	0.11	5.36

Comparisons of the classic models and proposed model for lane-by-lane field data on the M25 motorway were carried out to evaluate the model. Figure 5 shows the classic models and the proposed model fitted to field lane-by-lane data from M25/4068A. As seen in Figure 5, the performance of the various models is different. Compared to the Underwood model and the proposed model, the Greenshields and Van Aerde models did not perform as well for the lane-by-lane field data, which did not accurately predict the traffic speed–flow relationship in free-flow and congested-flow situations on the M25 motorway. Visually, our proposed model was able to better predict the turning point of the traffic speed–flow relationship in comparison with the Underwood model.
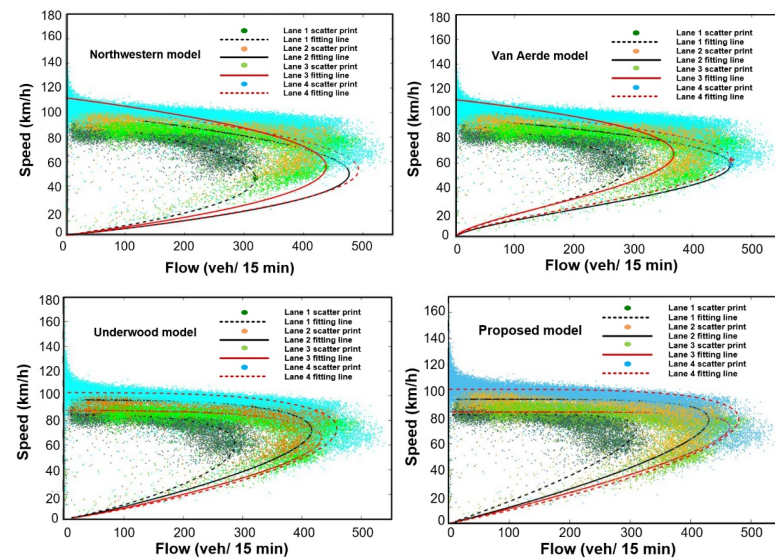

Figure 5. Performance of the classic models and our proposed model fitted to lane-by-lane field data from M25/4068A.

To evaluate quantitatively the goodness-of-fit of different models fitted to the lane-by-lane speed–flow relationship on the M25 motorway, the R^2 values were calculated. The results of the four best models are summarised in Table 5. Overall, the proposed model consistently achieved higher R^2 values compared to other models across all lanes on the

M25 motorway. Among the classic models, while the Underwood performed relatively well, the proposed model demonstrated superior accuracy and robustness, with a minimum R^2 of 0.79 and better fitting results, particularly in lane 1. The minimum R^2 across 20 datasets was 0.79 for lane 4 at the M25/4865 site, and lane 1 presented better fitting results compared to the other three lanes.

Table 5. R^2 values of fitting to lane-by-lane data (from Lane 1 to Lane 4) using the classic model and our proposed model.

Data Sites	Greenshields				Van Aerde				Underwood				The Proposed Model			
	R^2				R^2				R^2				R^2			
	L1	L2	L3	L4	L1	L2	L3	L4	L1	L2	L3	L4	L1	L2	L3	L4
M25/4055A	0.31	0.33	0.39	0.34	0.35	0.51	0.40	0.34	0.71	0.73	0.66	0.65	0.83	0.88	0.85	0.86
M25/4076A	0.61	0.49	0.52	0.36	0.67	0.56	0.52	0.54	0.64	0.51	0.49	0.48	0.92	0.84	0.86	0.80
M25/4097A	0.35	0.44	0.53	0.40	0.35	0.50	0.61	0.40	0.81	0.81	0.73	0.78	0.88	0.83	0.85	0.83
M25/4120A	0.41	0.48	0.42	0.42	0.42	0.57	0.44	0.45	0.72	0.76	0.66	0.73	0.84	0.83	0.85	0.82
M25/4139A	0.36	0.41	0.48	0.53	0.36	0.48	0.48	0.53	0.68	0.63	0.59	0.55	0.88	0.86	0.83	0.83
M25/4164A	0.49	0.54	0.54	0.45	0.49	0.60	0.54	0.42	0.84	0.87	0.69	0.68	0.96	0.89	0.91	0.89
M25/4193A	0.17	0.36	0.43	0.35	0.17	0.41	0.43	0.45	0.67	0.75	0.51	0.50	0.82	0.81	0.83	0.82
M25/4229A	0.25	0.45	0.39	0.54	0.26	0.50	0.39	0.39	0.78	0.80	0.69	0.69	0.90	0.86	0.85	0.80
M25/4259A	0.26	0.36	0.42	0.65	0.26	0.50	0.39	0.42	0.76	0.63	0.64	0.58	0.91	0.90	0.88	0.81
M25/4277A	0.20	0.30	0.33	0.32	0.22	0.37	0.41	0.41	0.64	0.72	0.46	0.51	0.82	0.83	0.89	0.87
M25/4296A	0.22	0.29	0.31	0.39	0.22	0.34	0.36	0.39	0.86	0.89	0.77	0.72	0.91	0.93	0.90	0.86
M25/4315A	0.20	0.31	0.31	0.37	0.20	0.35	0.41	0.38	0.81	0.76	0.68	0.68	0.91	0.89	0.90	0.88
M25/4332A	0.29	0.34	0.34	0.44	0.31	0.38	0.38	0.44	0.74	0.77	0.59	0.56	0.86	0.88	0.90	0.79
M25/4358A	0.26	0.29	0.35	0.47	0.26	0.34	0.42	0.47	0.73	0.73	0.59	0.60	0.80	0.83	0.85	0.83
M25/4390A	0.20	0.18	0.27	0.46	0.20	0.19	0.30	0.46	0.75	0.70	0.66	0.62	0.87	0.83	0.80	0.86
M25/4409A	0.30	0.30	0.48	0.36	0.30	0.32	0.48	0.45	0.68	0.63	0.63	0.70	0.80	0.82	0.83	0.83
M25/4423A	0.62	0.33	0.04	0.38	0.62	0.37	0.04	0.37	0.82	0.80	0.66	0.63	0.91	0.87	0.89	0.82
M25/4442A	0.22	0.31	0.40	0.42	0.24	0.39	0.40	0.41	0.79	0.78	0.75	0.80	0.87	0.81	0.80	0.80
M25/4465A	0.20	0.24	0.30	0.38	0.20	0.28	0.30	0.46	0.84	0.75	0.79	0.78	0.88	0.82	0.82	0.81
M25/4479A	0.24	0.39	0.34	0.32	0.24	0.27	0.34	0.31	0.66	0.66	0.60	0.76	0.80	0.85	0.91	0.87

In addition, the relative error and *RMSE* were also calculated to assess the performance of various applied models fitted to the lane-by-lane data on the M25 motorway. The results of relative error and *RMSE* are illustrated in Figures 6 and 7. It can be seen from Figures 6 and 7 that the relative error and *RMSE* of the proposed speed–flow model are generally lower than those of the other four models. The results of various model performances in terms of relative error and *RMSE* varied across various observation sites. The calculated relative error and *RMSE* varied when model parameters were set differently, but this had no significant effect on model performance. These results indicate that the proposed model accurately matched four-lane and lane-by-lane field data on the congested M25 motorway.
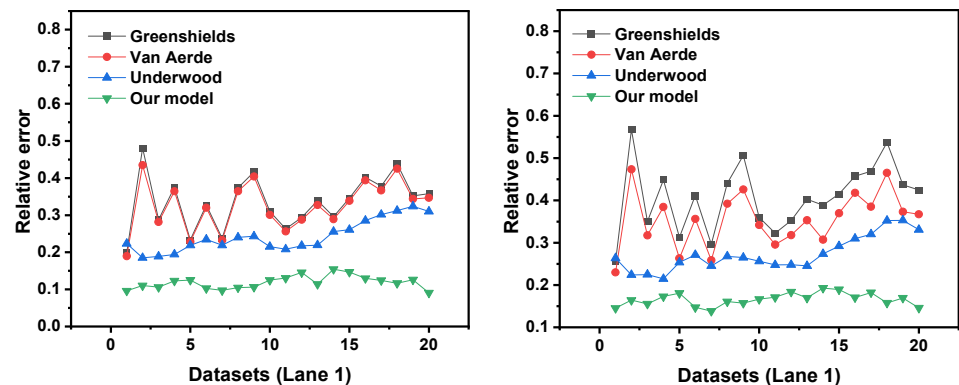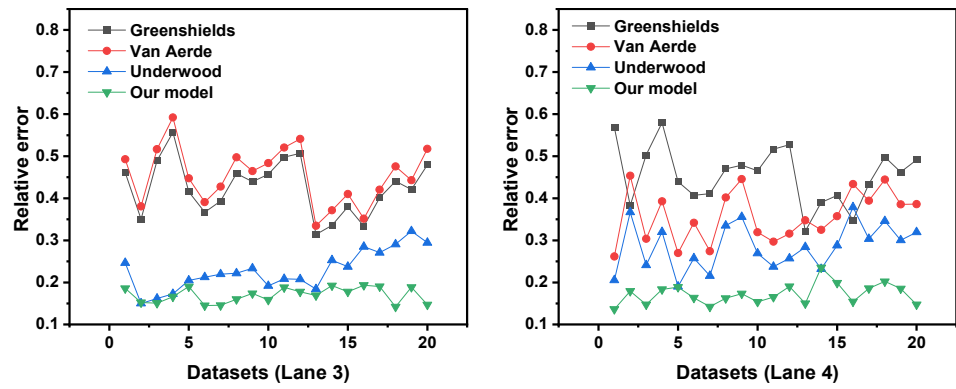

Figure 6. *Cont.*

Figure 6. Relative errors of different models fitted to lane-by-lane field data from various sites on the M25 motorway.
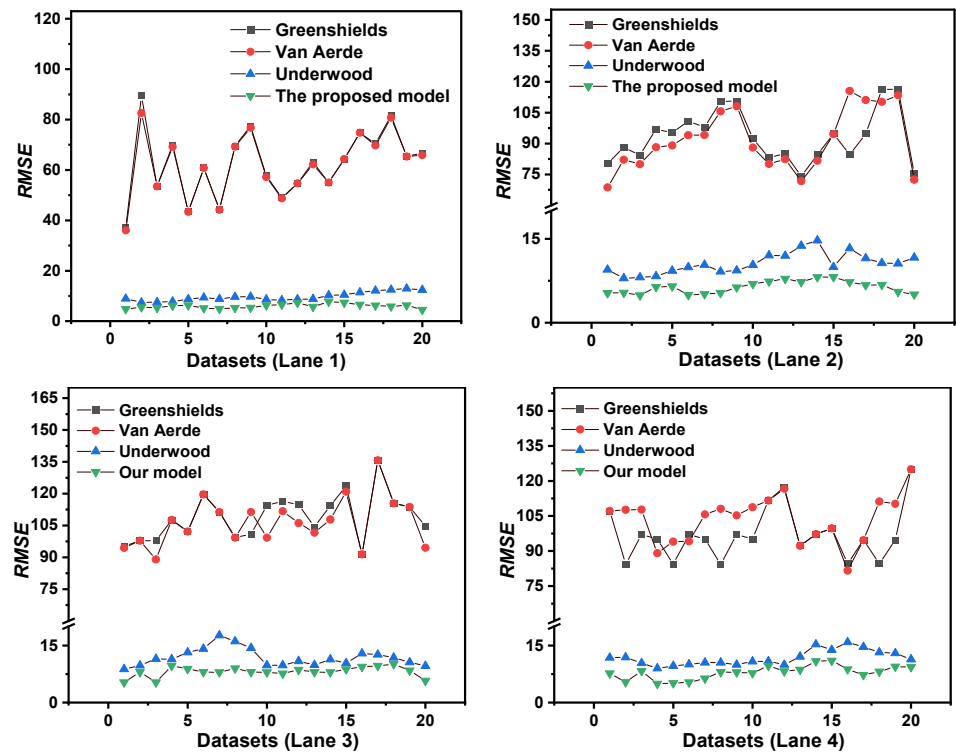

Figure 7. Root mean-squared error (RMSE) of different models fitted to lane-by-lane field data from various sites on the M25 motorway.

All the work in this section was based on our proposed model. Figure 8 shows the relationship between speed and flow using our proposed model under different weather conditions, including normal weather, light rain, and heavy rain. The normal weather data were the field data, while the speed and flow data under light and heavy rain were based on the average values of the previous studies shown in Table 2. The average reduction of speed under light and heavy rain was 5% and 7%, respectively, and the flow reduced by 7% and 11% on average, as used in the present work. Comparatively, Hranac et al. [14] reported reductions of 2% to 3.6% in free-flow speed under light rain and 6% to 9% under heavy rain, with a consistent capacity reduction of 10% to 11% across rainfall intensities. Additionally, rainfall caused a consistent reduction in capacity by 10% to 11%, irrespective of intensity. Akin et al. [15] observed speed reductions of 8% to 12% (approximately 7–8 km/h) and capacity decreases of 7% to 8% on urban freeways in Istanbul. Xu et al. [16] further highlighted the effects of rainfall on urban road networks, noting average reductions of 9.7% in weighted flow and 10.7% in weighted speed during the rainy evening peak.
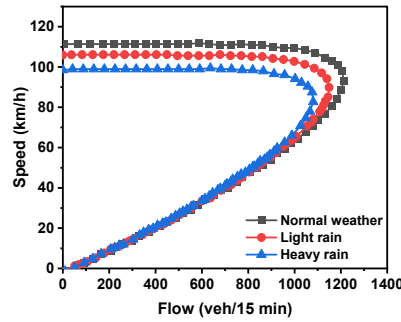
Figure 8. Speed–flow relationship using our proposed model under different weather conditions.

National Highways used the MIDAS system to automatically activate signals on the motorway network, aiming to delay the onset of traffic flow breakdown according to the CM algorithm. This algorithm primarily relies on traffic flow. When traffic flow approaches the road's capacity, marked as flow threshold (FT2), 60 mph signals are displayed to manage traffic and maintain smoother flow. If traffic flow continues to rise and reaches the flow threshold (FT3), the signals are adjusted to 50 mph. These thresholds (FT2 and FT3) were determined by National Highways at various locations on the M25. To explore potential relationships between the flow value at the turning point of the real speed–flow curve and FT2 and FT3, the data above were randomly selected, and a Gaussian function was employed to establish these relationships [51], as illustrated in Equations (5) and (6). The R^2 values for the relationships between the flow values at the turning point and FT2, as well as FT3, are 0.91 and 0.89, respectively. These results indicate that Equations (5) and (6) effectively capture the correlations between the flow values at the turning point and FT2/FT3. Given the change in the turning point of the traffic-flow curve under light and heavy rain conditions, the corresponding FT2 and FT3 thresholds of the CM algorithm should be adjusted.

$$FT2 = 1542 \exp(-\left(\frac{F_T - 1854}{1104}\right)^2) \tag{5}$$

$$FT3 = 1669 \exp(-\left(\frac{F_T - 1962}{1326}\right)^2) \tag{6}$$

where F_T is the traffic flow at the turning point.

Figure 9 depicts the thresholds of the CM algorithm under different weather conditions on the site M25/4229A. It should be noted that the M25/4229A was randomly selected as a representative example. The dashed line represents FT2 and the dotted line represents FT3. It can be seen that the values of traffic flow and speed of FT2 and FT3 under rainy days were smaller than the normal weather, which means that congestion management should be triggered in advance under rainfall conditions.
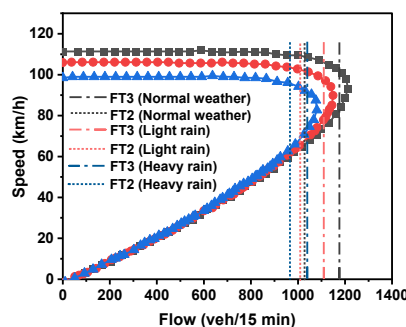

Figure 9. FT2 and FT3 values under different weather conditions.

5. Conclusions

This study proposed a single-regime speed–flow model, which was successfully fitted to the four-lane and lane-by-lane speed–flow relationships on the congested M25 motorway in England. The results demonstrated that the proposed model outperformed existing classic models, as indicated by smaller relative error and RMSE values and larger R^2 values. It means that the proposed model effectively captured the speed–flow relationship under both free-flow and congested-flow conditions, accurately matching field data from the M25 motorway. Furthermore, the developed model was applied to capture the impact of rainfall on the speed–flow relationship, revealing that both free-flow speed and road capacity experienced significant reductions under rainfall conditions. Heavy rain had a more pronounced effect compared to light rain. On this basis, a Gaussian function was utilised to determine the thresholds of the congestion management (CM) algorithm under various weather conditions. It was found that the thresholds of the congestion management algorithm were reduced under rain conditions. The results suggest that rainy days should be triggered at smaller thresholds in advance in the UK's intelligent congestion management system. Future research should focus on analysing extensive data from other congested motorways in England to evaluate the broader applicability of these findings.

References

1. Cohen, S.; Zhang, M.-Y. New speed flow relationships for road network planning in the Paris Region. In *Traffic And Transportation Studies (2002)*; American Society of Civil Engineers: Reston, VA, USA, 2002; pp. 389–396.
2. Karami, Z.; Kashef, R. Smart transportation planning: Data, models, and algorithms. *Transp. Eng.* **2020**, *2*, 100013. [CrossRef]
3. Khodabandelou, G.; Kheriji, W.; Selem, F.H. Link traffic speed forecasting using convolutional attention-based gated recurrent unit. *Appl. Intell.* **2021**, *51*, 2331–2352. [CrossRef]
4. Taylor, N.; Bourne, N.; Notley, S.; Skrobanski, G. Evidence for speed flow relationships. In *Proceedings of the European Transport Conference, Noordwijkerhout, The Netherlands, 6–8 October 2008*; Leeuwenhorst: Noordwijkerhout, The Netherlands, 2008; pp. 6–8.
5. Abou-Rahme, N.F. A Probabilistic Model for the Origin of Motorway Shockwaves. Ph.D. Thesis, University of Southampton, Southampton, UK, 2004.
6. Cassidy, M.J.; Bertini, R.L. Some traffic features at freeway bottlenecks. *Transp. Res. Part B Methodol.* **1999**, *33*, 25–42. [CrossRef]
7. Dailisan, D.N.; Lim, M.T. Agent-based modeling of lane discipline in heterogeneous traffic. *Phys. A Stat. Mech. Its Appl.* **2016**, *457*, 138–147. [CrossRef]

8. Kesting, A.; Treiber, M.; Schönhof, M.; Kranke, F.; Helbing, D. Jam-avoiding adaptive cruise control (ACC) and its impact on traffic dynamics. In *Traffic and Granular Flow*; Springer: Berlin/Heidelberg, Germany, 2007; pp. 633–643.

9. Mohan, R.; Ramadurai, G. Multi-class traffic flow model based on three dimensional flow–concentration surface. *Phys. A Stat. Mech. Its Appl.* **2021**, *577*, 126060. [CrossRef]

10. Xin, W.; Moonam, H.; Ala, M.V. *Connected Eco-Driving Technologies for Adaptive Traffic Signal Control*; New York State Energy Research and Development Authority: New York, NY, USA, 2019.

11. Diakaki, C.; Papageorgiou, M.; Papamichail, I.; Nikolos, I. Overview and analysis of vehicle automation and communication systems from a motorway traffic management perspective. *Transp. Res. Part A Policy Pract.* **2015**, *75*, 147–165. [CrossRef]

12. Vijayaraghavan, V.; Rian Leevinson, J. Intelligent traffic management systems for next generation IoV in smart city scenario. In *Connected Vehicles in the Internet of Things*; Springer: Berlin/Heidelberg, Germany, 2020; pp. 123–141.

13. Department of Transport, Road Traffic Statistics. 2024. Available online: https://roadtraffic.dft.gov.uk/manualcountpoints/27923?utm_source=chatgpt.com (accessed on 10 January 2025).

14. Hranac, R.; Sterzin, E.; Krechmer, D.; Rakha, H.A.; Farzaneh, M. *Empirical Studies on Traffic Flow in Inclement Weather*; Federal Highway Administration: Washington, DC, USA, 2006.

15. Akin, D.; Sisiopiku, V.P.; Skabardonis, A. Impacts of weather on traffic flow characteristics of urban freeways in Istanbul. *Procedia-Soc. Behav. Sci.* **2011**, *16*, 89–99. [CrossRef]

16. Xu, F.; He, Z.; Sha, Z.; Zhuang, L.; Sun, W. Assessing the impact of rainfall on traffic operation of urban road network. *Procedia-Soc. Behav. Sci.* **2013**, *96*, 82–89. [CrossRef]

17. Salvi, K.A.; Kumar, M.; Hainen, A.M. Sensitivity of Traffic Speed to Rainfall. *Weather Clim. Soc.* **2022**, *14*, 1165–1175. [CrossRef]

18. Nguyen, Y.-L.T.; Nguyen Duc, K.; Le, A.-T.; Nghiem, T.-D.; Than, H.-Y.T. Impact of real-world driving characteristics on the actual fuel consumption of motorcycles and implications for traffic-related air pollution control in Vietnam. *Fuel* **2022**, *345*, 128256. [CrossRef]

19. Yang, S.; Qian, S. Understanding and Predicting Travel Time with Spatio-Temporal Features of Network Traffic Flow, Weather and Incidents. *IEEE Intell. Transp. Syst. Mag.* **2019**, *11*, 12–28. [CrossRef]

20. Greenshields, B.; Bibbins, J.; Channing, W.; Miller, H. *A Study of Traffic Capacity, Highway Research Board Proceedings*; National Research Council (USA), Highway Research Board: Washington, DC, USA, 1935.

21. Pipes, L.A. Car Following Models and the Fundamental Diagram of Road Traffic. *Transp. Res.* **1966**, *1*, 21–29.

22. Drew, D.R. *Deterministic Aspects of Freeway Operations and Control*; Texas Transportation Institute: College Station, TX, USA, 1965.

23. Jayakrishnan, R.; Tsai, W.K.; Chen, A. A dynamic traffic assignment model with traffic-flow relationships. *Transp. Res. Part C Emerg. Technol.* **1995**, *3*, 51–72. [CrossRef]

24. Underwood, R.T. Speed, volume and density relationships. In *Quality and Theory of Traffic Flow*; Yale Bureau of Highway Traffic: New Haven, CT, USA, 1961; pp. 141–188.

25. Newell, G.F. Nonlinear effects in the dynamics of car following. *Oper. Res.* **1961**, *9*, 209–229. [CrossRef]

26. Swidler, J.C. *Northeast Power Failure, November 9 and 10, 1965: A Report to the President*; Federal Power Commission: Washington, DC, USA, 1965.

27. Kerner, B.S.; Konhäuser, P. Structure and parameters of clusters in traffic flow. *Phys. Rev. E* **1994**, *50*, 54. [CrossRef] [PubMed]

28. Wang, H.; Li, J.; Chen, Q.-Y.; Ni, D. Logistic modeling of the equilibrium speed–density relationship. *Transp. Res. Part A Policy Pract.* **2011**, *45*, 554–566. [CrossRef]

29. Greenberg, H. An analysis of traffic flow. *Oper. Res.* **1959**, *7*, 79–85. [CrossRef]

30. Van Aerde, M. Single regime speed-flow-density relationship for congested and uncongested highways. In Proceedings of the 74th Annual Meeting of the Transportation Research Board, Washington, DC, USA, 22–28 January 1995.

31. Edie, L.C. Car-following and steady-state theory for noncongested traffic. *Oper. Res.* **1961**, *9*, 66–76. [CrossRef]

32. Drake, J.; Schofer, J.; May, A. A statistical analysis of speed-density hypotheses; Traffic Flow and Transportation. *HRR* **1967**, *154*, 53–87.

33. Transportation Research Board. *Highway Capacity Manual*; HCM2010; Transportation Research Board, National Research Council: Washington, DC, USA, 2010; p. 1207.

34. May, A.D. *Traffic Flow Fundamentals*; Prentice Hall: Hoboken, NJ, USA, 1990.

35. Lei, Y.Z.; Gong, Y.; Yang, X.T. Unraveling stochastic fundamental diagrams considering empirical knowledge: Modeling, limitation and further discussion. *arXiv* **2024**, arXiv:2404.09318.

36. Cheng, Z.; Wang, X.; Chen, X.; Trépanier, M.; Sun, L. Bayesian calibration of traffic flow fundamental diagrams using Gaussian processes. *IEEE Open J. Intell. Transp. Syst.* **2022**, *3*, 763–771. [CrossRef]

37. Chin, S.M.; Franzese, O.; Greene, D.L.; Hwang, H.L.; Gibson, R. *Temporary Losses of Highway Capacity and Impacts on Performance: Phase 2*; United States Department of Energy Office of Scientific and Technical Information: Oak Ridge, TN, USA, 2004.

38. Rakha, H.; Farzaneh, M.; Arafeh, M.; Sterzin, E. Inclement weather impacts on freeway traffic stream behavior. *Transp. Res. Rec.* **2008**, *2071*, 8–18. [CrossRef]

39. Heshami, S.; Kattan, L.; Gong, Z.; Aalami, S. Deterministic and stochastic freeway capacity analysis based on weather conditions. *J. Transp. Eng. Part A Syst.* **2019**, *145*, 04019016. [CrossRef]

40. Datla, S.; Sharma, S. Impact of cold and snow on temporal and spatial variations of highway traffic volumes. *J. Transp. Geogr.* **2008**, *16*, 358–372. [CrossRef]

41. Agarwal, M.; Maze, T.H.; Souleyrette, R. Impacts of weather on urban freeway traffic flow characteristics and facility capacity. In Proceedings of the 2005 Mid-Continent Transportation Research Symposium, Ames, IA, USA, 18–19 August 2005.

42. Chung, Y. Assessment of non-recurrent congestion caused by precipitation using archived weather and traffic flow data. *Transp. Policy* **2012**, *19*, 167–173. [CrossRef]

43. Maze, T.H.; Agarwal, M.; Burchett, G. Whether weather matters to traffic demand, traffic safety, and traffic operations and flow. *Transp. Res. Rec.* **2006**, *1948*, 170–176. [CrossRef]

44. Jensen, T.C. *Weather and road capacity. Danish Journal of Transportation Research-Dansk Tidskrift for Transportforskning*; Aalborg University: Aalborg, Denmark, 2014.

45. Zhang, X.; Chen, M. Quantifying the impact of weather events on travel time and reliability. *J. Adv. Transp.* **2019**, *2019*, 8203081. [CrossRef]

46. Brilon, W.; Lohoff, J. Speed-flow Models for Freeways. *Procedia Soc. Behav. Sci.* **2011**, *16*, 26–36. [CrossRef]

47. Jin, S.; Wang, D.-h.; Xu, C.; Ma, D.-F. Short-term traffic safety forecasting using Gaussian mixture model and Kalman filter. *J. Zhejiang Univ. Sci. A* **2013**, *14*, 231–243. [CrossRef]

48. Kuang, Y.; Qu, X.; Wang, S. A tree-structured crash surrogate measure for freeways. *Accid. Anal. Prev.* **2015**, *77*, 137–148. [CrossRef]

49. Wang, D.; Ma, X.; Ma, D.; Jin, S. A Novel Speed–Density Relationship Model Based on the Energy Conservation Concept. *IEEE Trans. Intell. Transp. Syst.* **2017**, *18*, 1179–1189. [CrossRef]

50. Weng, J.; Meng, Q. Modeling speed-flow relationship and merging behavior in work zone merging areas. *Transp. Res. Part C: Emerg. Technol.* **2011**, *19*, 985–996. [CrossRef]

51. Liu, Y.; Chen, H.; Wu, S.; Yin, C.; Jiang, R.; Michalaki, V.; Rowley, G. Enhancement of traffic management algorithms for UK motorways. *Transp. Res. Procedia* **2023**, *72*, 1568–1575. [CrossRef]